Int. J. Heat Mass Transfer. Vol. 33, No. 8, pp. 1587–1597, 1990
Printed in Great Britain

0017-9310/90 $3.00+0.00

Thermal dispersion in a porous medium

C. T. HSU
Fluid Mechanics Department, TRW Space and Technology Group, Redondo Beach, CA 90278, U.S.A.

and

P. CHENG
Department of Mechanical Engineering, University of Hawaii, Honolulu, HI 96822, U.S.A.

(*Received* 9 *June* 1989 *and in final form* 21 *August* 1989)

Abstract—The thermal dispersion conductivity tensor for convection in a porous medium is derived based on the method of volume averaging of the velocity and temperature deviations in the pores. The velocity and temperature deviations are obtained based on flow over a dilute array of spheres, incorporated with a scale analysis. A multiplying constant (i.e. the thermal dispersivity tensor) is introduced to account for the interaction of spheres. Separate considerations are given to the creeping flow at low Reynolds numbers, as well as boundary layer flow and wakes at high Reynolds numbers. It is found that the velocity and porosity dependencies in the thermal dispersion conductivity tensor are different for high Reynolds number and low Reynolds number porous media flows. The value of the transverse thermal dispersivity for a nearly parallel flow at high Reynolds numbers is determined by comparing the predicted heat transfer characteristics with existing experimental results for forced convection of water and air through heated packed channels and cylindrical packed tubes.

INTRODUCTION

IT HAS been well established in the chemical engineering literature that thermal dispersion effects play an important role on forced convection in porous media [1–5]. Experiments on forced convection in packed columns have shown that the average radial or transverse thermal dispersion conductivity at high Reynolds numbers can be correlated as a linear function of Reynolds number [1–5], i.e.

$$(k'_T)_{av}/k_f = C_T\, Pe_m \tag{1}$$

where $(k'_T)_{av}$ is the cross-sectional average of the radial thermal dispersion conductivity; k_f the stagnant thermal conductivity of the fluid; $C_T = 0.09 \sim 0.1$ [4, 5]; Pe_m the Peclet number defined as $Pe_m = Re_d\, Pr_f = u_m d_p/\alpha_f$ (with $Pr_f = \nu_f/\alpha_f$ being the Prandtl number of the fluid and Re_d the Reynolds number based on the particle diameter d_p and the mean velocity u_m). From early experiments [1, 2, 5], it has been observed that steep radial temperature gradients exist near the heated or cooled wall in the packed columns. These steep temperature gradients were attributed to the channeling effect in early work [6].

In a series of papers, Cheng *et al.* [7–14] have analyzed the phenomena of steep temperature gradients in forced convection in a packed column by taking into consideration the effects of thermal dispersion, variable porosity, and nonuniform velocity distribution. In their analyses, the porosity distribution is approximated by an exponential function of the form [15]

$$\phi = \phi_\infty[1 + C_1 \exp(-N_1 y/d_p)] \tag{2}$$

where y is the distance from the wall; d_p the particle diameter, $\phi_\infty = 0.4$ the porosity of the bed away from the wall; $N_1 = 2$ and $C_1 = 1$ are the empirical constants used in most of the early work [7–12, 15–17], while the values of $N_1 = 5 \sim 6$ and $C_1 = 1$ were used in more recent work [12–14, 18]. Based on the correlation given by equation (1), Cheng *et al.* [7–14] assumed that the local transverse thermal dispersion conductivity k'_T is

$$k'_T/k_f = D_T\, Pe_m l(u/u_m) \tag{3}$$

where the factor u/u_m is introduced to account for the local velocity variation. In equation (3) l is a dimensionless dispersive length (normalized with respect to d_p) which was represented by a two-layer model [7, 8] in early work and is modeled as the Van Driest type of wall function in more recent work [9–13]. The Van Driest type of wall function is given by

$$l = 1 - \exp[-y/\omega d_p] \tag{4}$$

where ω is an empirical constant. Cheng *et al.* [7, 10] found that without the wall function in equation (3) the observed steep radial temperature gradients from experiments cannot be reproduced in theory. This implies that the channeling effect alone is not responsible for the observed temperature gradient behavior. The empirical constant D_T in equation (3) and ω in equation (4) were obtained by comparing the predicted heat transfer characteristics with experimental data. Thus, the values of D_T and ω depend on the values of N_1 and C_1 used in equation (2). The fol-

NOMENCLATURE

A area of fluid–solid interface
a, b Ergun's constants
B body force per unit volume
C_p specific heat at constant pressure
c_0, c_0', c_0'' constants defined in equations (26) and (28)
c_1 constant defined in equation (26)
C_1 constant defined in equation (2)
C_D drag coefficient defined in equation (23a)
C_T constant defined in equation (1)
D thermal dispersivity tensor
$D^{(n)}$ drag force for the nth sphere
D_T constant defined in equation (3)
d_p particle diameter
F inertial coefficient
$\mathbf{f}$ dimensionless vector function defined in equation (50)
$\mathbf{F}$ dimensionless vector function defined in equation (57)
$\mathbf{g}$ dimensionless vector function defined in equation (22)
$\mathbf{g}'$ dimensionless vector function defined in equation (52)
$\mathbf{G}$ dimensionless vector function defined in equation (25)
$\mathbf{G}'$ dimensionless vector function defined in equation (56)
H half width of a packed channel
i, j, k unit vectors in the x-, y- and z-directions
K permeability
k_d stagnant thermal conductivity of the fluid saturated porous medium
k_f thermal conductivity of the fluid phase
k_r radial thermal dispersion conductivity of the packed column
k_s thermal conductivity of the solid phase
k_T' local radial thermal dispersion conductivity
l wall function or dispersive length
n outward unit vector of a surface
N number of spheres in an elementary volume
N_1 constant defined in equation (2)
p pressure
Pe_m Peclet number defined in equation (1)
Pr_f Prandtl number of the fluid phase
r radial coordinate
r_0 radius of a packed column
R radius of a sphere
Re_{id} local Reynolds number based on particle diameter and the local average pore velocity
Re_d Reynolds number based on particle diameter and the mean velocity
S surface
T temperature
t time
u_m mean velocity in a packed column
V elementary volume
v velocity
W any physical quantity
x, y, z rectangular coordinates.

Greek symbols
α thermal diffusivity
μ dynamic viscosity of the fluid phase
ν kinematic viscosity of the fluid phase
ρ density
ϕ porosity of the packed bed
ω dimensionless constant defined in equation (4).

Subscripts
av average quantity
f quantity associated with the fluid phase
s quantity associated with the solid phase
α quantity associated with the α-phase
β quantity associated with the β-phase
∞ quantity at infinity.

Superscripts
$*$ dimensionless quantity
$\bar{}$ spatial average quantity
$'$ deviation quantity.

lowing values of D_T and ω were obtained for the best match between theory and experiments [9–13]:

(i) $D_T = 0.17$ and $\omega = 1.5$ if $N_1 = 2$ and $C_1 = 1$, and

(ii) $D_T = 0.12$ and $\omega = 1.0$ if $N_1 = 5$ and $C_1 = 1.4$.

Although theoretical results based on this *ad hoc* approach (i.e. equations (3) and (4)) agree with a number of experimental results, the approach lacks a rigorous mathematical basis, and is therefore subject to criticism.

In this paper, the thermal dispersion conductivity tensor for porous media flow is derived more rigorously from a volume averaging of the velocity and temperature deviations in the pores. The closure schemes for the thermal dispersion conductivity tensor are obtained based on the model of flow over a dilute random array of spheres. Explicit expressions of the thermal dispersion conductivities (within a multiplying constant) for high and low Reynolds number flows are obtained in terms of the Peclet number and a factor taking into consideration the local porosity variation in an approximate manner. The value of the transverse thermal dispersivity for high Reynolds

number flows is obtained by comparing the predicted heat transfer characteristics with existing experimental data for forced convection of air ($Pr = 0.7$) through an annular [5] and a cylindrical packed column under constant heat flux [3] or constant wall temperature [19] conditions. The approach was also applied to the problems of thermally developing forced convection of water ($Pr = 5.5$) through a packed channel where experimental data is available [20].

THE METHOD OF VOLUME AVERAGING

The macroscopic conservation equations for convective heat transfer in a porous medium can be obtained by a volume averaging of the microscopic conservation equations over a representative volume [21–26]. In this section, a brief discussion of the volume averaging process will be presented.

Consider a representative volume V in a porous medium consisting of an α-phase and a β-phase. If W_α is a quantity associated with the α-phase, an intrinsic phase average of W_α is defined as [21, 22]

$$\bar{W}_\alpha = \frac{1}{V_\alpha}\int_{V_\alpha} W_\alpha \, dV \tag{5}$$

where the volumetric integration is to be carried out over $dV = dx'\,dy'\,dz'$ with (x', y', z') denoting the microscopic coordinates. In equation (5) V_α is the volume occupied by the α-phase in V, and $V_\alpha + V_\beta = V$, with V_β being the volume occupied by the β-phase in V.

To derive the macroscopic equations from the microscopic equations, the following averaging theorems similar to those obtained by Whitaker [21] and Slattery [22] relating the volume average of a spatial derivative to the spatial derivative of the volume average are needed:

$$\frac{1}{V}\int_{V_\alpha} \nabla W_\alpha \, dV = \bar{\nabla}\left[\frac{1}{V}\int_{V_\alpha} W_\alpha \, dV\right] + \frac{1}{V}\int_{A_{\alpha\beta}} W_\alpha \, d\mathbf{S} \tag{6a}$$

$$\frac{1}{V}\int_{V_\alpha} \nabla\cdot\mathbf{W}_\alpha \, dV = \bar{\nabla}\cdot\left[\frac{1}{V}\int_{V_\alpha} \mathbf{W}_\alpha \, dV\right] + \frac{1}{V}\int_{A_{\alpha\beta}} \mathbf{W}_\alpha\cdot d\mathbf{S} \tag{6b}$$

where $A_{\alpha\beta}$ is the interface between the α- and β-phase in V, $d\mathbf{S}$ is a surface vector, and W_α and $\mathbf{W}_\alpha$ are a scalar and a vector, respectively. In equation (6), we differ from the previous work [21, 22] by distinguishing the gradient operators in the microscopic (x', y', z') and macroscopic coordinates (x, y, z) by ∇ and $\bar{\nabla}$ which are defined as

$$\nabla = \mathbf{i}\frac{\partial}{\partial x'} + \mathbf{j}\frac{\partial}{\partial y'} + \mathbf{k}\frac{\partial}{\partial z'} \tag{7a}$$

$$\bar{\nabla} = \mathbf{i}\frac{\partial}{\partial x} + \mathbf{j}\frac{\partial}{\partial y} + \mathbf{k}\frac{\partial}{\partial z}. \tag{7b}$$

Equation (6) can easily be obtained by applying the gradient and divergence theorems to a representative control volume V.

THE MACROSCOPIC CONTINUITY EQUATIONS

The microscopic continuity equation for an incompressible flow is given by

$$\nabla\cdot\mathbf{v}_f = 0 \tag{8}$$

where $\mathbf{v}_f$ is the microscopic velocity vector. Integrating equation (8) with respect to a representative volume in a porous medium, dividing the resulting expression by V and with the aid of equation (6b) yields

$$\bar{\nabla}\cdot(\phi\bar{\mathbf{v}}_f) = 0 \tag{9a}$$

where $\phi = V_f/V$ is the porosity while $\bar{\mathbf{v}}_f$ is the volumetric average (macroscopic) velocity vector. Equation (9a) can be rewritten as

$$\bar{\nabla}\cdot(\mathbf{v}) = 0 \tag{9b}$$

where $\mathbf{v} = \phi\bar{\mathbf{v}}_f$ is the Darcy velocity vector.

THE MACROSCOPIC MOMENTUM EQUATION

The microscopic momentum equation for an incompressible flow in a porous medium is given by the Navier–Stokes equation

$$\rho_f\left[\frac{\partial\mathbf{v}_f}{\partial t} + \nabla\cdot(\mathbf{v}_f\mathbf{v}_f)\right] = -\nabla p_f + \mu_f\nabla^2\mathbf{v}_f \tag{10}$$

where ρ_f and μ_f are the density and viscosity of the fluid while p_f is the pressure of the fluid. Integrating the above equation with respect to a representative volume and with the aid of equation (6) gives

$$\rho_f\left[\frac{\partial}{\partial t}(\phi\bar{\mathbf{v}}_f) + \bar{\nabla}\cdot(\phi\bar{\mathbf{v}}_f\bar{\mathbf{v}}_f)\right] = -\bar{\nabla}(\phi\bar{p}_f) + \mu_f\bar{\nabla}^2(\phi\bar{\mathbf{v}}_f) + \mathbf{B} \tag{11a}$$

where

$$\mathbf{B} = -\frac{1}{V}\int_{A_{fs}} p_f \, d\mathbf{S} + \frac{\mu_f}{V}\int_{A_{fs}} (\nabla\mathbf{v}_f)\cdot d\mathbf{S} \tag{11b}$$

which is the total drag force per unit volume (body force) due to the presence of the solid particles.

We now decompose the microscopic velocity vector $\mathbf{v}_f$ into the sum of the intrinsic phase average (macroscopic) velocity vector $\mathbf{v}_f$ and a deviation velocity vector $\mathbf{v}_f'$ [23], i.e.

$$\mathbf{v}_f = \bar{\mathbf{v}}_f + \mathbf{v}_f'. \tag{12}$$

It can be shown that

$$\overline{\mathbf{v}_f\mathbf{v}_f} = \bar{\mathbf{v}}_f\bar{\mathbf{v}}_f + \overline{\mathbf{v}_f'\mathbf{v}_f'}. \tag{13}$$

Substituting equation (13) into equation (11a) gives

$$\rho_f\left[\frac{\partial}{\partial t}(\phi\bar{\mathbf{v}}_f) + \bar{\nabla}\cdot(\phi\bar{\mathbf{v}}_f\bar{\mathbf{v}}_f) + \bar{\nabla}\cdot(\phi\overline{\mathbf{v}_f'\mathbf{v}_f'})\right] = -\bar{\nabla}(\phi\bar{p}_f) + \mu_f\bar{\nabla}^2(\phi\bar{\mathbf{v}}_f) + \mathbf{B}. \tag{14}$$

The second term on the left-hand side of equation (14) represents the macroscopic inertia force which is usually less important as compared to the terms on the right-hand side of equation (14) where the pressure gradient is balanced by the body force over the entire porous media, except near the wall for which the Brinkman's frictional effect predominates. The third term on the left-hand side of equation (14) represents the hydrodynamic dispersion which is of higher order as compared to the second term on the left-hand side of equation (14), and can therefore be neglected. Thus, equation (14), in terms of the Darcy velocity, reduces to

$$\rho_f\left[\frac{\partial\mathbf{v}}{\partial t} + \bar{\nabla}\cdot\left(\frac{\mathbf{v}\cdot\mathbf{v}}{\phi}\right)\right] = -\bar{\nabla}p + \mu_f\bar{\nabla}^2\mathbf{v} + \mathbf{B} \tag{15}$$

where $p = \phi\bar{p}_f$.

CLOSURE MODELING FOR THE DRAG FORCE DUE TO SOLID PARTICLES

To obtain closures for the body force term **B**, we now consider flow past a dilute random array of spheres (i.e. spheres with negligible interaction) with a macroscopic velocity vector $\mathbf{v}_f$. If the representative volume V contains N spheres of diameter d_p (or radius R), equation (11b) becomes

$$\mathbf{B} = N\mathbf{D}^{(n)}/V \tag{16}$$

where

$$\mathbf{D}^{(n)} = -\int_{A_{fs}^{(n)}} p_f^{(n)}\,d\mathbf{S} + \mu_f\int_{A_{fs}^{(n)}}\nabla\mathbf{v}_f^{(n)}\cdot d\mathbf{S} \tag{17}$$

represents the drag force on the nth sphere. In equation (17), $p_f^{(n)}$ and $\mathbf{v}_f^{(n)}$ are the local pressure and velocity in the flow field around the nth sphere. The macroscopic pressure $\bar{p}_f$ and velocity $\bar{\mathbf{v}}_f$ can now be regarded as the ambient condition. With the quasi-steady state assumption [26], the momentum equation for $\mathbf{v}_f^{(n)}$ according to equation (10) is

$$\rho_f(\mathbf{v}_f^{(n)}\cdot\nabla)\mathbf{v}_f^{(n)} = -\nabla p_f^{(n)} + \mu_f\nabla^2\mathbf{v}_f^{(n)}. \tag{18}$$

We now introduce the following dimensionless variables:

$$\mathbf{v}_f^* = \mathbf{v}_f^{(n)}/|\bar{\mathbf{v}}_f|,\quad p_f^* = (p_f^{(n)} - \bar{p}_f)/\rho_f|\bar{\mathbf{v}}_f|^2$$
$$(x^*, y^*, z^*) = (x'/d_p, y'/d_p, z'/d_p). \tag{19}$$

Equation (18), in terms of these dimensionless variables, becomes

$$(\mathbf{v}_f^*\cdot\nabla^*)\mathbf{v}_f^* = -\nabla^* p_f^* + \frac{1}{Re_{fd}}\nabla^{*2}\mathbf{v}_f^* \tag{20}$$

where

$$\nabla^* = \mathbf{i}\frac{\partial}{\partial x^*} + \mathbf{j}\frac{\partial}{\partial y^*} + \mathbf{k}\frac{\partial}{\partial z^*}$$

is the dimensionless gradient operator, and $Re_{fd} = |\bar{\mathbf{v}}_f|d_p/\nu_f$ is the Reynolds number based on particle diameter and average pore velocity. The boundary conditions for $\mathbf{v}_f^*$ are

$$\mathbf{v}_f^* = 0 \quad \text{on the surface of the sphere} \tag{21a}$$

and

$$\mathbf{v}_f^* = \bar{\mathbf{v}}_f/|\bar{\mathbf{v}}_f| = \mathbf{i}_v \quad \text{away from the sphere} \tag{21b}$$

where $\mathbf{i}_v$ is a unit vector in the $\bar{\mathbf{v}}_f$ direction.

DRAG FORCE FOR HIGH REYNOLDS NUMBER FLOWS ($Re_{fd} \gg 10$)

At high Reynolds number flow ($Re_{fd} \gg 10$), there exists a viscous boundary layer of $O(Re_{fd}^{-1/2})$ at the proximity of the spherical wall. Outside the viscous boundary layer, the viscous terms are less important and they represent a higher order correction to the potential flow produced by the balance between the advection and pressure terms. Solutions to equations (20) and (8) subject to boundary conditions (21) at high Reynolds number can be found in the open literature. In this study, it is sufficient to give a general expression of the solution outside the boundary layer in the polar coordinates (r^*, θ) as

$$\mathbf{v}_f^* = \mathbf{g}(r^*, \theta) + O(Re_{fd}^{-1/2}) \tag{22}$$

where $\mathbf{g}$ satisfies $\mathbf{g}(\infty, \theta) = \mathbf{i}_v$ and $\mathbf{g}(1/2, \theta) = \mathbf{t}(\theta)$ with $\mathbf{t}$ being a vector tangential to the surface of the sphere.

To evaluate the drag force on the sphere, the boundary layer solution to equations (20) and (21) is needed. For this purpose, equation (20) will now be expressed in terms of a new scale $\eta^* = (r^* - 1/2)Re_{fd}^{1/2}$. The drag force can then be obtained through a matched asymptotic expansion procedure [28] to give

$$\mathbf{D}^{(n)} = C_D\frac{d_p^2}{2}\rho_f|\bar{\mathbf{v}}_f|^2\mathbf{i}_v \tag{23a}$$

where

$$C_D = \frac{6\pi}{Re_{fd}^{1/2}}[c_0' + c_1'\,Re_{fd}^{-1/2} + O(Re_{fd}^{-1})]. \tag{23b}$$

The zero order term in equation (23b) is due to the skin friction while the first order correction is due to the form drag associated with the stagnation flow near the leading edge.

Drag force for low Reynolds number flows ($Re_{fd} \ll 10$)

At low Reynolds numbers ($Re_{fd} \ll 10$), the viscous effect is significant for the entire flow field. The pressure generated in a creeping flow depends not only on the flow velocity but also on the viscosity. The proper scale for pressure is $\mu_f|\bar{\mathbf{v}}_f|/d_p$ and the dimensionless pressure is given by $p_f'^* = (p_f^{(n)} - \bar{p}_f)d_p/\mu_f|\bar{\mathbf{v}}_f| = p_f^* Re_{fd}$. Equation (20), in terms of this dimensionless pressure, becomes

$$Re_{fd}(\mathbf{v}_f^* \cdot \nabla^*)\mathbf{v}_f^* = -\nabla^* p_f'^* + \nabla^{*2}\mathbf{v}_f^*. \tag{24}$$

The solution to equation (24) for low Reynolds number flow can be expressed in the form

$$\mathbf{v}_f^* = \mathbf{G}(r^*, \theta) + O(Re_{fd}) \tag{25}$$

where $\mathbf{G}(r^*, \theta)$ satisfies the boundary condition $\mathbf{G}(1/2, \theta) = 0$. For low Reynolds number flow, the drag force is contributed from both the pressure drag and skin friction, and the result for the drag coefficient is given by

$$C_D = \frac{6\pi}{Re_{fd}}[c_0 + c_1\, Re_{fd} + O(Re_{fd}^2)] \tag{26}$$

where the zero order term is the Stokes drag and the first order correction is Oseen's correction associated with the inertial terms in equation (24).

Composite expression for the drag force

From equation (26) it is observed that at low Reynolds number flow, the drag coefficient is dominated by $6\pi c_0/Re_{fd}$ associated with the Stokes drag, and the inertial force represents a first order correction which is given by $6\pi c_1$. Equation (23) shows that as the Reynolds number is increased, the skin friction of the laminar boundary layer becomes dominant with a drag coefficient of $6\pi c_0'/Re_{fd}^{1/2}$ and, at the same time, the Stokes drag is degenerated to a stagnation form drag near the leading edge of the sphere with additional drag coefficient given by $6\pi c_1'/Re_{fd}$. If the Reynolds number is increased further, the flow is expected to separate from the surface of the sphere to form a wake. The drag force associated with the wake is predominated by the inertial effect of the flow with a constant drag coefficient, i.e.

$$C_D = 6\pi c_0''. \tag{27}$$

Combining equations (23), (26) and (27), we write the drag coefficient as

$$C_D = 6\pi(c_0/Re_{fd} + c_0'/Re_{fd}^{1/2} + c_0''). \tag{28}$$

Substituting equations (23) and (28) into equation (16) yields

$$\mathbf{B} = -\frac{18(1-\phi)}{d_p^2}[c_0 + c_0'\, Re_{fd}^{1/2} + c_0''\, Re_{fd}]\mu_f|\bar{\mathbf{v}}_f|\mathbf{i}_v \tag{29a}$$

where we have used the geometric relation

$$4\pi R^3 N/3V = 1-\phi. \tag{29b}$$

In equation (29a) c_0, c_0' and c_0'' are constants. Equation (29b), with $c_0 = a(1-\phi)/18\phi$, $c_0' = 0$ and $c_0'' = b/18$, reduces to Ergun's expression

$$\mathbf{B} = -\left[\frac{\mu_f\phi\mathbf{v}}{K} + \rho_f\frac{F\phi\mathbf{v}|\mathbf{v}|}{\sqrt{K}}\right] \tag{30}$$

where $\mathbf{v} = \phi\bar{\mathbf{v}}_f$ is the Darcy velocity, $K = \phi^3 d_p^2/a(1-\phi)^2$ and $F = b/\sqrt{a}\phi^{3/2}$, with a and b being the Ergun constants. It follows from equations (15) and (30) that the macroscopic momentum equation for an incompressible flow in a variable porosity medium is

$$\rho_f\left[\frac{\partial\mathbf{v}}{\partial t} + \nabla\cdot\left(\frac{\mathbf{v}\cdot\mathbf{v}}{\phi}\right)\right] = -\nabla p + \mu_f\nabla^2\mathbf{v} - \left[\frac{\mu_f\phi\mathbf{v}}{K} + \rho_f\frac{F\phi\mathbf{v}|\mathbf{v}|}{\sqrt{K}}\right]. \tag{31}$$

THE MACROSCOPIC ENERGY EQUATION

The microscopic energy equations for the fluid and solid phases are

$$(\rho C_p)_f\left[\frac{\partial T_f}{\partial t} + \nabla\cdot(\mathbf{v}_f T_f)\right] = \nabla\cdot(k_f\nabla T_f) \tag{32a}$$

and

$$(\rho C_p)_s\frac{\partial T_s}{\partial t} = \nabla\cdot(k_s\nabla T_s) \tag{32b}$$

where the interface conditions are

$$T_f = T_s \quad \text{on } A_{fs} \tag{33a}$$

$$\mathbf{n}_{fs}\cdot k_f\nabla T_f = \mathbf{n}_{fs}\cdot k_s\nabla T_s \quad \text{on } A_{fs}. \tag{33b}$$

With the aid of equation (6), a volume averaging of equation (32) gives

$$\frac{\partial}{\partial t}[\phi(\rho C_p)_f\bar{T}_f] + (\rho C_p)_f\bar{\nabla}\cdot[\phi\overline{\mathbf{v}_f T_f}] = \bar{\nabla}\cdot[k_f\bar{\nabla}(\phi\bar{T}_f)] + \bar{\nabla}\cdot\left[\frac{1}{V}\int_{A_{fs}} k_f T_f\, d\mathbf{S}\right] + \frac{1}{V}\int_{A_{fs}} k_f\nabla T_f\cdot d\mathbf{S} \tag{34a}$$

and

$$\frac{\partial}{\partial t}[(1-\phi)(\rho C_p)_s\bar{T}_s] = \bar{\nabla}\cdot[k_s\bar{\nabla}(1-\phi)\bar{T}_s] - \bar{\nabla}\cdot\left[\frac{1}{V}\int_{A_{fs}} k_s T_s\, d\mathbf{S}\right] - \frac{1}{V}\int_{A_{fs}} k_s\nabla T_s\cdot d\mathbf{S} \tag{34b}$$

where $(\rho C_p)_f$ and $(\rho C_p)_s$ are the heat capacities of the fluid and the solid phases; T_f and T_s the fluid and solid temperatures which are related to their intrinsic phase temperatures $\bar{T}_f$ and $\bar{T}_s$ by

$$\bar{T}_f = \frac{1}{V_f}\int_{V_f} T_f \, dV$$

$$\bar{T}_s = \frac{1}{V_s}\int_{V_s} T_s \, dV. \tag{35}$$

The quantity $\overline{\mathbf{v}_f T_f}$ in equation (34a) is defined as

$$\overline{\mathbf{v}_f T_f} = \frac{1}{V_f}\int_{V_f} \mathbf{v}_f T_f \, dV. \tag{36}$$

Adding equations (34a) and (34b) and with the aid of boundary condition (33b) yields

$$\frac{\partial}{\partial t}[\phi(\rho C_p)_f \bar{T}_f + (1-\phi)(\rho C_p)_s \bar{T}_s] + (\rho C_p)_f \bar{\nabla}\cdot[\phi\overline{\mathbf{v}_f T_f}] = \bar{\nabla}\cdot\{k_f \bar{\nabla}(\phi \bar{T}_f) + k_s \bar{\nabla}[(1-\phi)\bar{T}_s]\} + \bar{\nabla}\cdot\left[\frac{1}{V}\int_{A_{fs}} (k_f T_f - k_s T_s)\, dS\right]. \tag{37}$$

We now decompose T_f and T_s as [26]

$$T_f = \bar{T}_f + T_f'$$

$$T_s = \bar{T}_s + T_s'. \tag{38}$$

At this point, we make use of the local thermal equilibrium assumption [26], i.e.

$$\bar{T}_f = \bar{T}_s = \bar{T}. \tag{39}$$

Substituting equations (13) and (38) into equation (37) and with the aid of equation (39) leads to

$$\frac{\partial}{\partial t}[\phi(\rho C_p)_f + (1-\phi)(\rho C_p)_s]\bar{T} + (\rho C_p)_f \bar{\nabla}\cdot[\phi(\bar{\mathbf{v}}_f \bar{T} + \overline{\mathbf{v}_f' T_f'})] = \bar{\nabla}^2[\phi k_f + (1-\phi)k_s]\bar{T} + \bar{\nabla}\cdot\left[\frac{1}{V}\int_{A_{fs}} (k_f T_f' - k_s T_s')\, dS\right] \tag{40a}$$

where

$$\overline{\mathbf{v}_f' T_f'} = \frac{1}{V_f}\int_{V_f} \mathbf{v}_f' T_f' \, dV \tag{40b}$$

represents the thermal dispersion effect. Nozad *et al.* [25] showed that the terms on the right-hand side of equation (40b) can be closed by

$$\bar{\nabla}^2[\phi k_f + (1-\phi)k_s]\bar{T} + \bar{\nabla}\cdot\left[\frac{1}{V}\int_{A_{fs}} (k_f T_f' - k_s T_s')\, dS\right] = \bar{\nabla}\cdot(k_d \bar{\nabla}\bar{T}) \tag{41}$$

where k_d is the stagnant thermal conductivity of the saturated porous medium. Equation (40a), with equation (41), reads

$$\frac{\partial}{\partial t}[\phi(\rho C_p)_f + (1-\phi)(\rho C_p)_s]\bar{T} + (\rho C_p)_f \bar{\nabla}\cdot[\phi(\bar{\mathbf{v}}_f \bar{T} + \overline{\mathbf{v}_f' T_f'})] = \bar{\nabla}\cdot(k_d \bar{\nabla}\bar{T}) \tag{42}$$

which is the macroscopic energy equation for convection in a porous medium.

CLOSURE MODELING FOR THERMAL DISPERSION

We now discuss the closure modeling for thermal dispersion given by equation (40b), using the model of flow over a dilute array of spheres similar to those obtained for the body force as discussed in the previous sections. To this end, we first rewrite equation (40b) as

$$\overline{\mathbf{v}_f' T_f'} = \frac{N}{V_f}\int_{V_f^{(n)}} \mathbf{v}_f'^{(n)} T_f'^{(n)} \, dV \tag{43}$$

where $V_f^{(n)}$ is the volume enclosing the nth sphere. In equation (43), $\mathbf{v}_f'^{(n)}$ and $T_f'^{(n)}$ are the local velocity and temperature deviations in the flow field near the nth sphere which are given by

$$\mathbf{v}_f'^{(n)} = \mathbf{v}_f^{(n)} - \bar{\mathbf{v}}_f \tag{44a}$$

$$T_f'^{(n)} = T_f^{(n)} - \bar{T}_f \tag{44b}$$

with $T_f^{(n)}$ denoting the local temperature in the pore. With the aid of the geometric relation (29), equation (43) can be rewritten as

$$\overline{\mathbf{v}_f' T_f'} = \frac{1-\phi}{\phi}\int_{V_f^{*(n)}} \mathbf{v}_f'^{(n)} T_f'^{(n)} \, dV^* \tag{45}$$

where $V_f^{*(n)} = V_f^{(n)}/(4\pi R^3/3)$ is the dimensionless volume enclosing the nth sphere. It is important to note that equation (45) contains a factor $(1-\phi)/\phi$ which takes into consideration the local pore geometry. To evaluate the integral in equation (45), a solution for $T_f'^{(n)}$ is needed in addition to $\mathbf{v}_f'^{(n)}$ which is given by equations (21) and (25).

To obtain the governing equation for $T_f'^{(n)}$, we note that the microscopic energy equation for $T_f^{(n)}$ is given by

$$(\rho C_p)_f \frac{\partial T_f^{(n)}}{\partial t} + (\rho C_p)_f \nabla\cdot(\mathbf{v}_f^{(n)} T_f^{(n)}) = \nabla\cdot(k_f \nabla T_f^{(n)}) \tag{46}$$

which is also the equation given by equation (32a). Substituting equation (44b) into equation (46) and subtracting equation (34a) divided by ϕ from the resulting equation yields

$$(\rho C_p)_f \left\{\frac{\partial T_f'^{(n)}}{\partial t} + \nabla\cdot[\mathbf{v}_f'^{(n)}\bar{T}_f + \bar{\mathbf{v}}_f T_f'^{(n)}] + \nabla\cdot[\mathbf{v}_f'^{(n)} T_f'^{(n)} - \overline{\mathbf{v}_f'^{(n)} T_f'^{(n)}}]\right\} = \nabla\cdot[k_f \nabla T_f'^{(n)}] - \bar{\nabla}\cdot\left[\frac{1}{V_f}\int_{A_{fs}} k_f T_f \, dS\right] - \frac{1}{V_f}\int_{A_{fs}} k_f \nabla T_f \cdot dS. \tag{47}$$

The last two nonlinear terms on the left-hand side of equation (47) are of higher order and can therefore be neglected. Using a scale argument and the quasi-steady assumption of Zanotti and Carbonell [26], equation (47) becomes

$$(\rho C_p)_f \nabla \cdot (\mathbf{v}_f^{\prime(n)} \bar{T}_f + \bar{\mathbf{v}}_f T_f^{\prime(n)}) = \nabla \cdot (k_f \nabla T_f^{\prime(n)}) - \left[\frac{1}{V_f} \int_{A_{fs}} k_f \nabla T_f^{\prime(n)} \cdot d\mathbf{S} \right] \quad (48)$$

where we have used the continuity equation, and the following integral results:

$$\int_{A_{fs}} \bar{T}_f \, d\mathbf{S} = \int_{A_{fs}} \nabla \bar{T}_f \cdot d\mathbf{S} = 0. \quad (49)$$

It is noted that the integral term on the right-hand side of equation (48) is a constant in the volume V_f. This constant is implicit in the conductive term. $\nabla \cdot [k_f \nabla T_f^{\prime(n)}]$. The combined result of the two terms on the right-hand side of equation (48) is to make the right-hand side a fluctuative quantity to justify physically with the left-hand side. Solution forms for $T_f^{\prime(n)}$ will now be considered for high and low Reynolds number flows so that explicit expressions for thermal dispersion given by the integral (43) can be evaluated.

THERMAL DISPERSION IN HIGH REYNOLDS NUMBER FLOW ($Re_{fd} \gg 10$)

At high Reynolds numbers ($Re_{fd} \gg 10$), terms on the right-hand side of equation (48) can be neglected as they are associated with heat conduction. A dimensional analysis (with d_p as the length scale of the microscopic coordinates) of the simplified equation gives

$$T_f^{\prime(n)} = d_p \mathbf{f}(\mathbf{r}') \cdot \nabla \bar{T} \quad (50)$$

where the macroscopic temperature gradient $\nabla \bar{T}$ has been considered as a constant in the microscopic coordinates and $\mathbf{f}(\mathbf{r}')$ is a dimensionless vector function depending on the microscopic coordinates ($\mathbf{r}'$), whose origin is at the center of the nth sphere.

From equation (21) the velocity near the nth sphere is given by

$$\mathbf{v}_f^{(n)} = |\bar{\mathbf{v}}_f| \mathbf{g}(\mathbf{r}') \quad (51)$$

$$\mathbf{v}_f^{\prime(n)} = \mathbf{v}_f^{(n)} - \mathbf{v}_f = |\bar{\mathbf{v}}_f| \mathbf{g}'(\mathbf{r}') \quad (52)$$

where $\mathbf{g}'(\mathbf{r}')$ is also a dimensionless vector function depending only on the microscopic coordinates. Substituting equations (50) and (52) into equation (45) yields

$$\phi \overline{\mathbf{v}_f' T_f'} = -\underline{\alpha}' : \nabla \bar{T} \quad (53)$$

where the thermal dispersion diffusivity tensor $\underline{\alpha}'$ is given by

$$\underline{\alpha}' = -(1-\phi)|\bar{\mathbf{v}}_f| d_p \int_{V_f^*} \mathbf{g}'(\mathbf{r}') \mathbf{f}(\mathbf{r}') \, dV^*. \quad (54)$$

Note that the integral in equation (54) is a dimensionless tensor which can be evaluated numerically. However, this is not necessary in view of the approximation of negligible interaction of spheres. To take this effect into account, we now replace the integral by an unknown dimensionless tensor $\underline{D}$ in equation (54) to give

$$\underline{\alpha}' = \underline{D}(1-\phi)|\bar{\mathbf{v}}_f| d_p = \underline{D} \frac{(1-\phi)}{\phi} |\bar{\mathbf{v}}| d_p. \quad (55a)$$

It follows from equation (55a) that the thermal dispersion conductivity tensor $\underline{k}'$ is given by

$$\underline{k}' = (\rho C_p)_f \underline{\alpha}' = \underline{D} k_f \frac{(1-\phi)}{\phi} \frac{|\bar{\mathbf{v}}| d_p}{\alpha_f} = \underline{D} k_f \frac{(1-\phi)}{\phi} Pe \quad (55b)$$

where $Pe = |\bar{\mathbf{v}}| d_p / \alpha_f$ is the Peclet number and the value of $\underline{D}$ can be determined by a comparison with experiments. Equation (55) shows that the thermal dispersion conductivity and thermal dispersion diffusivity at high Reynolds numbers are linearly proportional to the Peclet number, which is consistent with most of the existing experimental correlations [1–5].

THERMAL DISPERSION IN LOW REYNOLDS NUMBER FLOWS ($Re_{fd} \ll 10$)

The thermal dispersion conductivity tensor in low Reynolds number flow ($Re_{fd} \ll 10$) in a porous medium can be obtained in a similar manner. At low Reynolds numbers, where creeping flow prevails, the velocity deviation from equation (25) is

$$\mathbf{v}_f^{\prime(n)} = \mathbf{v}_f^{(n)} - \mathbf{v}_f = |\bar{\mathbf{v}}_f| \mathbf{G}'(\mathbf{r}') \quad (56)$$

where $\mathbf{G}'(\mathbf{r}')$ is a dimensionless vector function depending only on the local microscopic coordinates ($\mathbf{r}'$). At low Reynolds number flow, where heat conduction is predominant, a scale analysis of equation (48) shows that the temperature deviation in the pores is given by

$$T_f' = \frac{d_p^2}{\alpha_f} |\bar{\mathbf{v}}_f| \mathbf{F}(\mathbf{r}') \cdot \nabla \bar{T} \quad (57)$$

where $\nabla \bar{T}$ has been considered as a constant in the microscopic coordinates ($\mathbf{r}'$), and $\mathbf{F}(\mathbf{r}')$ is a dimensionless vector function depending only on the microscopic coordinates $\mathbf{r}'$. Equation (57) is the closure scheme derived by Carbonell and Whitaker [25] using another argument and assuming a periodic medium. Substituting equations (56) and (57) into equation (45) yields

$$\phi \overline{\mathbf{v}_f' T_f'} = -\underline{\alpha}' : \nabla \bar{T} \quad (58a)$$

where

$$\underline{\alpha}' = -(1-\phi) \frac{|\bar{\mathbf{v}}_f|^2 d_p^2}{\alpha_f} \int_{V_f^*} \mathbf{G}'(\mathbf{r}') \mathbf{F}(\mathbf{r}') \, dV^*. \quad (58b)$$

If the integral in equation (58) is replaced by an unknown tensor $\underline{\underline{D}}^*$, it follows that the thermal dispersion diffusivity tensor is given by

$$\underline{\underline{\alpha}}' = \underline{\underline{D}}^* \frac{(1-\phi)}{\phi^2} |\bar{v}|^2 d_p^2/\alpha_f \tag{59a}$$

and the thermal dispersion conductivity tensor $\underline{\underline{k}}'$ is

$$\underline{\underline{k}}' = (\rho C_p)_f \underline{\underline{\alpha}}' = k_f \underline{\underline{D}}^* \frac{(1-\phi)}{\phi^2} |\bar{v}|^2 d_p^2/\alpha_f^2$$

$$= k_f \underline{\underline{D}}^* \frac{(1-\phi)}{\phi^2} Pe^2 \tag{59b}$$

where $\underline{\underline{D}}^*$ is the thermal dispersivity tensor at low Reynolds number flow. Equation (59) shows that the thermal dispersion diffusivity and the thermal dispersion conductivity have a quadratic dependence on velocity. It is pertinent to point out that the velocity and porosity dependencies in the expressions given by equations (55) and (59) are different in the high and low Reynolds number flow regions. This is analogous to Darcian and Forchheimer's frictional terms which also have different velocity and porosity dependencies. It follows from equations (42), (53) and (58a) that the macroscopic energy equation for convection in a porous medium with the fluid/solid matrix in local thermal equilibrium is

$$\frac{\partial}{\partial t}[\phi(\rho C_p)_f + (1-\phi)(\rho C_p)_s]\bar{T} + (\rho C_p)_f \bar{\nabla} \cdot [\bar{v}\bar{T}]$$

$$= \bar{\nabla} \cdot (k_d \bar{\nabla}\bar{T} + \underline{\underline{k}}' : \bar{\nabla}\bar{T}). \tag{60}$$

FORCED CONVECTION IN CYLINDRICAL AND ANNULAR PACKED TUBES

A considerable amount of experimental work has been carried out for forced convection of air ($Pr = 0.7$) in cylindrical and annular packed tubes filled with glass spheres. In particular, Verschoor and Schuit [19] have conducted an experiment on forced convection of air in a cylindrical packed tube (having a diameter of 43 mm) with uniform temperature, while Quinton and Storrow [3] have performed another experiment on a similar geometry (having a diameter of 41.8 mm) with uniform heat flux. Yagi and Kunii [5] have performed experiments for forced convection of air in an annular packed tube heated asymmetrically. Analyses of these experimental data based on a hydrodynamically and thermally fully-developed flow incorporating the wall function given by equation (4) for radial thermal dispersion have been performed by Cheng and co-workers [9, 11]. In the following we shall solve the same problems using the thermal dispersion conductivity given by equation (55a). In all of the computations, the following values are used: $N_1 = 5$, $C_1 = 1$, $a = 215$ and $b = 1.92$. Note that for a hydrodynamically and thermally fully-developed flow in a packed tube or channel, the thermal dispersion conductivity tensor $\underline{\underline{k}}'$ reduces to a scalar which is the radial thermal dispersion conductivity k_r'. According to equation (55b) the radial thermal dispersion conductivity at high Reynolds numbers is given by

$$k_r' = D' \frac{(1-\phi)}{\phi} Pe_m \, k_f (u/u_m) \tag{61}$$

where ϕ is the porosity which is given by

$$\phi = \phi_\infty \{1 + C_1 \exp[-N_1(r_o - r)/d_p]\} \tag{62a}$$

for a cylindrical packed tube with radius r_o, and

$$\phi = \phi_\infty \{1 + C_1 \exp[-N_1(r_o - r)/d_p]\}$$

$$\times \{1 + C_1 \exp[-N_1(r - r_i)/d_p]\} \tag{62b}$$

for an annular packed tube with inner and outer radii r_i and r_o. In equation (61) u_m is the mean velocity in the packed tube; $Pe_m = u_m d_p/\alpha_f$ is the Peclet number based on u_m, while u are the axial dimensionless velocity profiles which were recomputed according to the methods described in the previous papers [7–13]. As in the previous work [7–13], the value of the radial thermal dispersivity D' will be determined by comparing the predicted heat transfer characteristics with appropriate experimental data. It was found that the predicted heat transfer characteristics would match the best with experimental data if the value of $D' = 0.04$ was used for numerical computations.

A comparison of theoretical and experimentally determined Nusselt numbers for a hydrodynamically and thermally fully-developed flow in a cylindrical packed tube with constant wall temperature and constant heat flux are presented in Figs. 1 and 2, respectively. It is shown that the theory and experiments are in good agreement with each other.

Figure 3 is a comparison of theoretical and experimental temperature distributions for a fully-developed forced convective flow in an annular

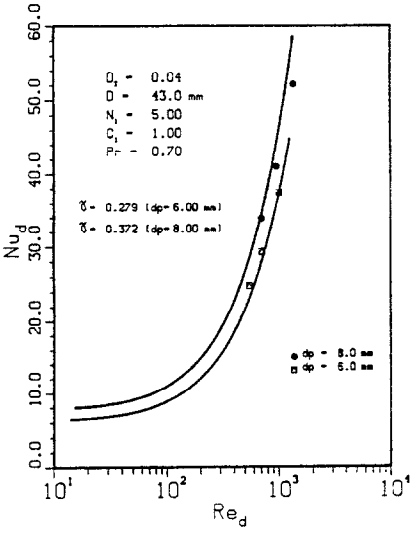

FIG. 1. Predicted and measured Nusselt numbers for forced convection of air in a cylindrical packed tube at constant wall temperature.

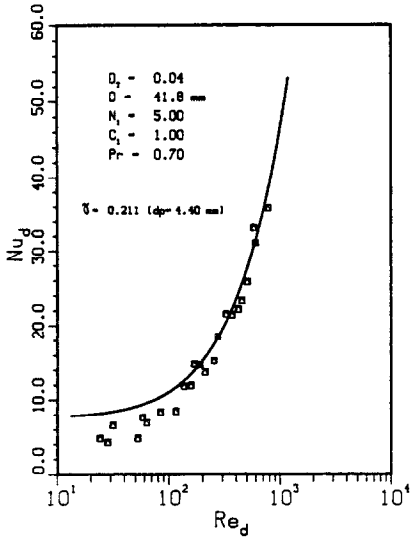

FIG. 2. Predicted and measured Nusselt numbers for forced convection of air in a cylindrical packed tube at constant heat flux.

packed column with $\gamma = d_p/r_i = 0.25$ and $Re_d = 131.4$. It is shown that the steep radial temperature gradient observed in the experiment is reproduced approximately by the present theory. Figure 4 shows the comparison of the predicted and measured Nusselt numbers vs Re_d for forced convection of air in the annular packed tube with different particle diameters. The predicted Nusselt numbers are shown to be lower than those obtained from experiments.

FORCED CONVECTION IN PACKED CHANNELS

The problem of a thermally developing forced convective flow in a packed channel heated asymmetrically has been considered previously by Cheng *et al.* [12] with the radial thermal dispersion conductivity

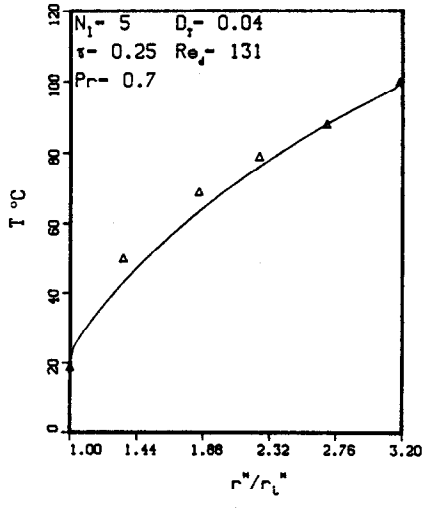

FIG. 3. Predicted and measured radial temperature distribution in an annular packed tube with asymmetric heating.

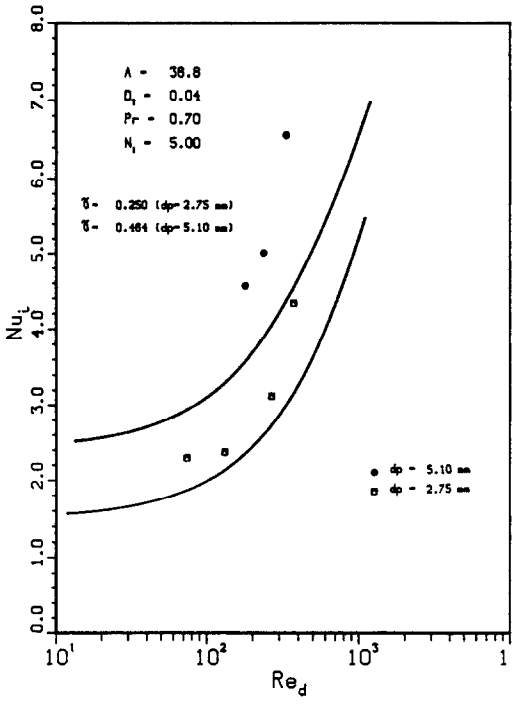

FIG. 4. Predicted and measured Nusselt numbers for forced convection of air in an annular packed tube with asymmetric heating.

given by equations (3) and (4). The same problem will now be considered based on the present theory, and the predicted temperature distributions will be compared with experimental data obtained by Schroeder *et al.* [20].

Figure 5 shows the predicted and experimentally determined temperature distributions for forced convection of water in a channel (with half width H) filled with two different sizes of glass spheres ($\gamma = 0.0741$ and 0.3704) at a location of $x/2H = 13.5$ for $Re_d = 405$ and 321. It is seen that the observed temperature gradients [20] are steeper than those predicted by the theory. For $\gamma = 0.3704$ the predicted temperature profile becomes almost linear, indicating a thermally fully-developed flow is attained at $x/2H = 13.5$. The agreement between theory and experiments for the case of $\gamma = 0.3704$ is not as good as those for $\gamma = 0.074$.

CONCLUDING REMARKS

The macroscopic equations for forced convection of an incompressible flow in a variable porosity medium are obtained based on a volume averaging of the microscopic equations. The thermal dispersion terms in the macroscopic energy equation are derived by a volume average of the spatial velocity and temperature derivations in the pores. With a scale analysis of the governing equations for temperature deviations, it is shown that the microscopic temperature deviations in the pores are expressible in

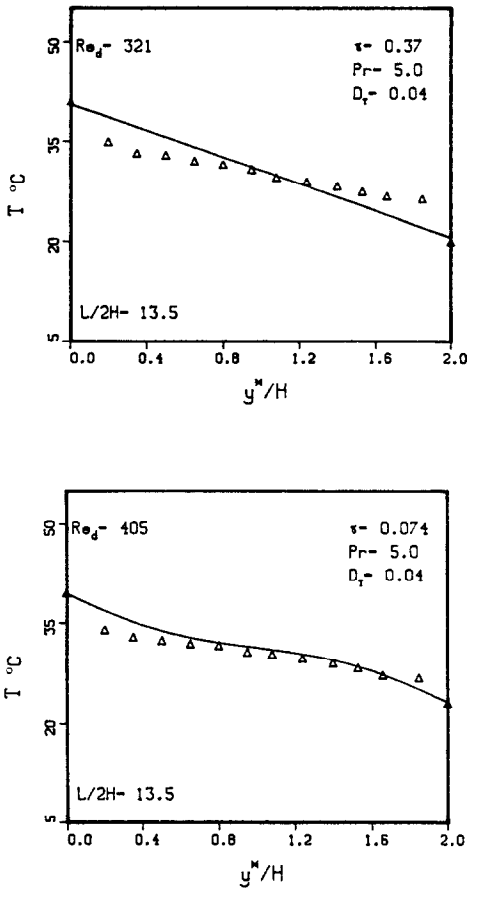

FIG. 5. Predicted and measured temperature distributions for forced convection of water in a packed channel with asymmetric heating.

terms of the macroscopic temperature gradient for both high and low Reynolds number flows. However, the resulting expressions for the thermal dispersion conductivities in the two flow regimes contain different porosity and Peclet number dependencies. The value of the thermal dispersivity tensor must be determined by a comparison of theory and experiments.

For a nearly parallel flow at high Reynolds numbers, the thermal dispersivity tensor reduces to a scalar, i.e. the transverse thermal dispersivity. Thus, the value of the transverse thermal dispersivity can be obtained by comparing the predicted heat transfer characteristics with experiments for forced convection in cylindrical and annular packed tubes. The theory is also applied to forced convection in a packed channel.

A preliminary version of the paper was published in ref. [14] which contains an algebraic error in the derivation of the thermal dispersion conductivity tensor. For this reason, equations (53)–(55) as well as (58), (59), and (61) of this paper differ from those presented in ref. [14] by a factor of ϕ. Consequently, the value of $D' = 0.04$ reported in this paper differs from the value of $D' = 0.02$ reported in ref. [14].

Acknowledgement—This work was supported by NSF Grant No. MSM87-14705.

REFERENCES

1. C. A. Coberly and W. R. Marshall, Jr., Temperature gradients in gas streams flowing through fixed granular beds, *Chem. Engng Prog.* **47**, 141–150 (1951).
2. D. A. Plautz and H. F. Johnstone, Heat and mass transfer in packed beds, *A.I.Ch.E. Jl* **1**, 193–199 (1955).
3. J. H. Quinton and J. A. Storrow, Heat transfer to air flowing through packed tubes, *Chem. Engng Sci.* **5**, 245–257 (1956).
4. S. Yagi and N. Wakao, Heat and mass transfer from wall to fluid in packed beds, *A.I.Ch.E. Jl* **5**, 79–85 (1959).
5. S. Yagi and D. Kunii, Studies on heat transfer near wall surface on packed tubes, *A.I.Ch.E. Jl* **6**, 97–104 (1960).
6. A. P. De Wasch and G. F. Froment, Heat transfer in packed beds, *Chem. Engng Sci.* **27**, 567–576 (1972).
7. P. Cheng and D. Vortmeyer, Transverse thermal dispersion and wall channelling in a packed bed with forced convective flow, *Chem. Engng Sci.* **9**, 2523–2532 (1988).
8. P. Cheng and C. T. Hsu, Fully-developed forced convective flow through an annular packed-sphere bed with wall effects, *Int. J. Heat Mass Transfer* **29**, 1843–1853 (1986).
9. P. Cheng and C. T. Hsu, Applications of Van Driest's mixing length theory to transverse thermal dispersion in forced convective flow through a packed bed, *Int. Commun. Heat Mass Transfer* **13**, 613–625 (1986).
10. P. Cheng, Wall effects on fluid flow and heat transfer in porous media, *Proc. 2nd ASME/JSME Thermal Engng Joint Conf.*, Vol. 2, pp. 297–303 (1987).
11. P. Cheng and H. Zhu, Effects of radial thermal dispersion on fully-developed forced convection in cylindrical packed tubes, *Int. J. Heat Mass Transfer* **30**, 2373–2383 (1987).
12. P. Cheng, C. T. Hsu and A. Chowdhury, Forced convection in the entrance region of a packed channel with asymmetric heating, *J. Heat Transfer* **110**, 946–954 (1988).
13. P. Cheng, Recent studies of wall effects on fluid flow and heat transfer in packed-sphere beds, *Proc. Indian Congress of Appl. Mech.* (1987).
14. C. T. Hsu and P. Cheng, Closure schemes of the macroscopic energy equation for convective heat transfer in porous media, *Int. Commun. Heat Mass Transfer* **15**, 689–703 (1988).
15. B. C. Chandrasekhara and D. Vortmeyer, Flow model for velocity distribution in fixed porous beds under isothermal conditions, *Fluid Dyn.* **12**, 105–111 (1979).
16. K. Vafai, Convective flow and heat transfer in variable-porosity media, *J. Fluid Mech.* **147**, 233–259 (1984).
17. D. Vortmeyer and J. Schuster, Evaluation of steady flow profiles in rectangular and circular packed beds by a variational method, *Chem. Engng Sci.* **38**, 1691–1699 (1983).
18. M. L. Hunt and C. L. Tien, Non-Darcian convection in cylindrical packed beds, *Proc. 2nd ASME/JSME Thermal Engng Conf.*, Vol. 2, pp. 433–438 (1987).
19. H. Verschoor and G. C. A. Schuit, Heat transfer to fluids flowing through a bed of granular solids, *Appl. Scient. Res.* **A2**, 97–119 (1952).
20. K. J. Schroeder, U. Renz and K. Elegeta, Forschungsberichte des Landes Nordrhein-Westfalen No. 3037 (1981).
21. S. Whitaker, Diffusion and dispersion in porous media, *A.I.Ch.E. Jl* **13**, 420–427 (1967).
22. J. C. Slattery, Flow of viscoelastic fluids through porous media, *A.I.Ch.E. Jl* **13**, 1066–1071 (1967).
23. W. G. Gray, A derivation of the equations for multiphase transport, *Chem. Engng Sci.* **30**, 229–233 (1975).

24. R. G. Nozad, R. G. Carbonell and S. Whitaker, Heat conduction in multiphase systems: I. Theory and experiment for two-phase systems, *Chem. Engng Sci.* **40**, 843–855 (1985).
25. R. G. Carbonell and S. Whitaker, Heat and mass transfer in porous media. In *Fundamentals of Transport Phenomena in Porous Media* (Edited by J. Bear and M. Y. Corapcioglu), pp. 121–198. Martinus Nijhoff, Dordrecht, The Netherlands (1984).
26. F. Zarotti and R. G. Carbonell, Development of transport equations for multiphase systems II, *Chem. Engng Sci.* **39**, 263–278 (1984).
27. S. Ergun, Fluid flow through packed columns, *Chem. Engng Prog.* **48**, 89–94 (1952).

DISPERSION THERMIQUE DANS UN MILIEU POREUX

Résumé—Le tenseur de conductivité de dispersion thermique pour la convection dans un milieu poreux est obtenu à partir de la méthode des volumes moyennant les déviations de vitesse et de température dans les pores. Ces déviations sont obtenues à partir de la solution externe pour l'écoulement autour d'un arrangement dilué de sphères, avec analyse dimensionnelle. Une constante multiplicative (le tenseur de dispersivité thermique) est introduite pour tenir compte de l'interaction des sphères. On considère aussi les écoulements rampants à faible nombre de Reynolds et l'écoulement de couche limite et des sillages à grand nombre de Reynolds. On trouve que la dépendance de la vitesse à la porosité dans le tenseur de conductivité de dispersion thermique est différente pour les écoulements dans les milieux poreux selon que le nombre de Reynolds est élevé on faible. La valeur de la dispersivité thermique transversale pour un écoulement parallèle à grand nombre de Reynolds est déterminée en comparant les caractéristiques de transfert thermique prédites aux résultats expérimentaux connus pour la convection forcée de l'eau et de l'air à travers des lits fixes chauds.

THERMISCHE DISPERSION IN EINEM PORÖSEN MEDIUM

Zusammenfassung—Der Tensor der Wärmeleitfähigkeit bei thermischer Dispersion wird für Konvektion in einem porösen Medium hergeleitet. Grundlage ist eine volumetrische Mittelwertsbildung der Temperatur- und Geschwindigkeitsschwankungen in den Poren. Diese Schwankungen ergeben sich aufgrund der äußeren Lösung für eine Strömung über eine verdünnte Anordnung von Kugeln unter Anwendung einer Dimensions- und Größenordnungsanalyse. Eine multiplikative Konstante (d. h. der Tensor der thermischen Dispersivität) wird eingeführt, um die Wechselwirkung der Kugeln zu berücksichtigen. Bei kleinen Reynolds-Zahlen wird die schleichende Strömung mit einbezogen, bei großen Reynolds-Zahlen die Grenzschichtströmung und die Wirbelgebiete. Es zeigt sich, daß die Einflüsse von Geschwindigkeit und Porosität im Wärmeleitfähigkeitstensor bei thermischer Dispersion unterschiedlich sind für hohe und für niedrige Reynolds-Zahlen der Strömung im porösen Medium. Der Wert der quergerichteten thermischen Dispersion wird für eine nahezu parallele Strömung bei hoher Reynolds-Zahl dadurch bestimmt, daß der berechnete Wärmeübergang mit vorhandenen experimentellen Ergebnissen für erzwungene Strömung von Wasser und Luft durch Festbettanordnungen verglichen wird.

РАССЕЯНИЕ ТЕПЛА В ПОРИСТОЙ СРЕДЕ

Аннотация—Для исследования конвекции в пористой среде методом усреднения отклонений скорости и температуры найден тензор теплопроводности. Отклонения скорости и температуры получены на основе внешнего решения для потока над рассредоточенной упаковкой сфер совместно с анализом размерностей и шкал. Для учета взаимодействия сфер вводится постоянный множитель (т.е. для тензора теплопроводности). Отдельно рассматриваются ползучий поток при низких значениях числа Рейнольдса, а также течение в пограничном слое и следы при высоких значениях числа Рейнольдса. Найдено, что зависимость компонент тензора теплопроводности от порозности и скорости различна для течений в пористых средах при высоких и низких значениях числа Рейнольдса. Значение поперечной теплопроводности в случае почти параллельного течения при высоких числах Рейнольдса определяется посредством сопоставления расчетных характеристик теплопереноса с имеющимися экспериментальными данными для вынужденной конвекции воды и воздуха через нагретые упакованные слои.